

# Influence of pinning centers of different natures on surrounding vortices

Rodolfo Carvalho dos Santos<sup>1</sup>, Elwis Carlos Sartorelli Duarte<sup>1</sup>, Danilo Okimoto<sup>1</sup>, Alice Presotto<sup>1</sup>, Edson Sardella<sup>2</sup>, Maycon Motta<sup>3</sup>, Rafael Zadorosny<sup>1</sup>

<sup>1</sup>Departamento de Física e Química, Universidade Estadual Paulista (UNESP), Faculdade de Engenharia, Caixa Postal 31, 15385-000, Ilha Solteira, SP, Brazil

<sup>2</sup>Departamento de Física, Universidade Estadual Paulista (UNESP), Faculdade de Ciências de Bauru, Caixa Postal 473, 17033-360, Bauru, SP, Brazil

<sup>3</sup>Departamento de Física, Universidade Federal de São Carlos (UFSCar), São Carlos, SP, Brazil

E-mail: rafael.zadorosny@unesp.br

May 2021

**Abstract.** Studies involving vortex dynamics and their interaction with pinning centers are an important ingredient to reach higher critical currents in superconducting materials. The vortex distribution around arrays of engineered defects, such as blind and through holes, may help to improve the superconducting properties. Thus, in this work, we used the time-dependent Ginzburg-Landau theory to investigate the vortex dynamics in superconductors of mesoscopic dimensions with a large central square defect with three different configurations: (i) a hole which passes through the sample (interface with the vacuum); (ii) a superconducting region with lower critical temperature ( $T_c$ ); and (iii) a region with a more robust superconductivity, i.e., with a higher  $T_c$ . Such systems can be envisaged as elementary building blocks of a macroscopic decorated specimen. Therefore, we evaluated the influence of different interfaces on the vortex dynamics and their effects in the field-dependent magnetization and time-dependent induced electric potential variation. The results show that the lower critical field is independent from the nature of the defect. However, the currents crowd at the vertices of the through hole producing a lower degradation of the local superconductivity, which may increase the upper critical field. On the other hand, the last type of defect can be used to control the vortex dynamics in the main superconducting region around the defect with more accuracy. Whereas the first two defects are attractive for the vortices, the third type is repulsive for them, being needed several vortices penetrated in the superconducting matrix to have vortices penetrated into it.

*Keywords:* vortex dynamics, TDGL, superconductivity, defects

Submitted to: *Supercond. Sci. Technol.*

## 1. Introduction

In type-II superconductors, the viscous motion of vortices generates a resistive state producing heat and might lead the material to the normal state. Then, vortices must be kept static to avoid the premature destruction of the superconductivity. One way to trap such fluxoids is the introduction of attractive potentials into the superconducting sea, the so-called pinning centers (PCs), which can maintain the vortices pinned against the Lorentz Force produced by both shielding and transport currents circulating around the material [1, 2]. On one hand, PCs consist of defects naturally present, which occurs during the material preparation, such as twin-boundaries [3], oxygen vacancies [4], and grain boundaries [5]. On the other hand, a variety of works have been reported the use of artificial PCs, randomly or regularly ordered, as the introduction of arrays of magnetic dots [6, 7] and through or blind holes [8, 9]. In several cases, lithographic techniques based on electron, ion, and neutron beam radiation have been used to produce both through holes, also know as antidots (ADs) [10, 11, 12], as well as blind holes (BHs) [13, 14, 15, 16, 17].

As a matter of fact, samples patterned with BHs present a pinning force weaker in comparison to specimens decorated with ADs [13, 18, 19]. Additionally, both vortex states and their interaction with the interfaces between the defect and the superconductor can be accessed. In Ref. [14], a Nb thin film was irradiated by reactive ion etching to form a regular array of circular BHs with radius in the range  $0.15 \mu\text{m} < R < 2.2 \mu\text{m}$ . The authors showed that the trapped vortices form a shell-like structure following the geometry of the defect. Moreover, the number of vortices that nucleate inside the hole is not sensitive to the thickness of the BHs. On the other hand, using the Ginzburg-Landau formalism [13], it was shown that different vortex states as dimer, trimer, and other shell-like structures, are available into the BHs depending on the number of trapped vortices. For large BHs ( $R = 6\xi(0)$ , where  $\xi(0)$  is the coherence length at zero temperature), the average distance between vortices depends on both the radius of that structure and the total number of vortices penetrated in the sample. Besides that, for very large BHs ( $R = 30\xi(0)$ ), vortices are arranged in an Abrikosov lattice at the center of the BH for vorticities counting hundreds of flux quanta. However, in the BH contour, the vortices form a shell-like distribution. The above-cited works showed that the vortices into the defects behave independently of those in the main superconducting matrix.‡ Furthermore, it is interesting to note that inside the BHs, the vortices experience confinement effects similar to those presented by mesoscopic systems [20, 21, 22, 23].

Concerning heterostructures with thickness modulation, Brisbois *et al.* [24] have fabricated by e-beam lithography two 140-nm thick Nb films with a central macroscopic defect shaped like a polygonal thickness step, one excavated with a thinner thickness (80 nm) and another one with a thicker central region (200 nm). In the former case, vortices

‡ By *superconducting matrix*, we mean the main region around the defect which is either a superconductor of lower or higher critical temperature ( $T_c$ ).

penetrate more profound due to the reduction of the thickness-dependent critical current in its thinner center, whereas in the latter, the thicker defect behaves as a barrier for the incoming fluxoids. Using the time-dependent Ginzburg-Landau (TDGL) formalism, the authors traced the vortex trajectories and confirmed these features. Moreover, these behaviors were also observed in abrupt flux penetration phenomena, the so-called flux avalanches, in which sudden bursts of ultrafast dendritic flux rush into the sample. Another way to substantially enhance the protection against avalanches consists of the addition of a thin Nb layer before the reactive deposition of NbN, thus forming a NbN/Nb hybrid [25].

In a recent work [26], the TDGL formalism was applied to study the vortex dynamics in thin and large superconducting films with a hexagonal array of PCs. The results were contrasted with experimental measurements of the critical current density of a patterned MoGe thin film. The effects of the pinning force were studied for different types of defects, their sizes, and displacement on the sample. It was shown that  $J_c(H)$  is defect-dependent, being higher for BHs with diameter  $d = 300$  nm, and a depth  $h = 300$  nm. Also, different vortex dynamics were associated with matching fields, i.e., the commensurability effects between the vortex lattice with the pinning lattice that enhances the critical current density [27].

Vortex pinning and matching fields were also reported in superconductors with *antipinning centers*, i.e., samples decorated with superconducting dots. In Ref. [28], an increase of the the authors described an increase of the critical current density,  $J_c$ , as a consequence of a vanadium film deposited on an array of Nb dots for temperatures below 3 K. Additionally, Gillijns and coworkers[29] deposited an array of Pb microrings over an Al film. For zero-field cooling measurements, the microrings repel the vortices to the interstitial pinning potentials; conversely, an attractive interaction between vortices and microrings takes place for field cooling processes. Such change of antipinning behavior was also reported by Carreira *et al.*[30] in Nb films with a triangular array of vanadium dots. Besides that, the equilibrium vortex configurations were described by Berdiyrov and coworkers [31] in the framework of Ginzburg-Landau theory. Pillars were considered as antipinning centers, and some theoretical results were experimentally demonstrated in Nb film etched with a square array of circular pillars. The authors showed that the radius and thickness of the pillars induces a plethora of vortex structures in the interstitial sites. Also, for larger pillars, vortices penetrate them forming shell structures by inducing the same symmetry to the interstitial ones.

In general, it is noted that studies of the vortex interaction with defects are an issue of great importance from fundamental to applied physics of the superconducting materials. Besides that, most used systems are in bulk or film forms, and confinement effects are present only inside the BH-like defects or antipinnings. Thus, in the present work, we simulated, using the TDGL formalism, square samples decorated with different square defects: an AD, a blind hole, and a strong dot. The first one is described as a superconducting matrix with a through hole in its center with superconducting-vacuum interfaces. The second and the third ones are composed of central superconducting

regions with a lower critical temperature ( $T_c$ ) and a higher  $T_c$ , respectively. Hence we focus our investigation on the influence of these different types of mesoscopic defects in the vortex matter of superconducting samples at the nanoscale.

## 2. Theoretical Formalism

In the TDGL formalism [32], the complex superconducting order parameter,  $\psi$ , and the magnetic vector potential,  $\mathbf{A}$ , are described as a function of time. Within such formalism, an electric potential  $\Phi$  can be taken into account. Thus, it is possible to study non-equilibrium states of the vortex matter. Those equations in dimensionless units are given by,

$$u\left(\frac{\partial}{\partial t} + i\Phi\right)\psi = (-i\nabla - \mathbf{A})^2\psi + (g(\mathbf{r}) - T - |\psi|^2)\psi, \quad (1)$$

$$\left(\frac{\partial \mathbf{A}}{\partial t} + \nabla\Phi\right) = \mathbf{J} - \kappa^2\nabla \times \nabla \times \mathbf{A}, \quad (2)$$

$$\mathbf{J} = \text{Re}(\psi^*(-i\nabla - \mathbf{A})\psi) \quad (3)$$

where  $\mathbf{J}$  is the superconducting current density. The function  $g(\mathbf{r})$  defines the defect regions. For  $g > 1$ , the defect is a superconducting material with  $T_c$  larger than that of the matrix, whereas for  $0 \leq g < 1$ , the local  $T_c$  is lower than that of the matrix;  $\kappa$  is the Ginzburg-Landau parameter defining the superconducting material. Equations (1), (2), and (3) are dimensionless, the distances are written in units of  $\xi(0)$ ; the fields in units of the upper critical field at zero temperature,  $H_{c2}(0)$ ;  $\mathbf{A}$  is in units of  $H_{c2}(0)\xi(0)$ , and time in units of the characteristic GL time,  $t_{GL}(0) = \frac{\pi\hbar}{8k_B T_c u}$ . Thus,  $u$  is the ratio between  $\frac{\tau_{|\psi|}}{t_{GL}}$ , where  $\tau_{|\psi|}$  is the relaxation time of  $|\psi|$ . Following the microscopic derivation of the TDGL equation presented by L. P. Gor'kov and G. M. Eliashberg [33],  $u = 12$  for a superconductor with large concentration of paramagnetic impurities. However, in situations where the studied phenomena are not sensible to the relaxation process, it can be set  $u = 1$  (or less) to minimize computational time [34, 35].

Considering a better analysis involving the interaction between vortex dynamics and mesoscopic defects, in this work, the time-dependence of the magnetization  $M(t)$ , induced voltage  $V(t)$ , and free energy  $E(t)$ , at non-equilibrium processes were studied. In normalized units, such equations are given as follows.

$$V = -\frac{\partial}{\partial t} \int_C \mathbf{A} \cdot d\mathbf{l}, \quad (4)$$

$$\mathbf{M} = \mathbf{B} - \mathbf{H}, \quad (5)$$

$$E = \left(\frac{1}{2}|\psi|^2 - (g(\mathbf{r}) - T)\right)|\psi|^2 + \left|(-i\nabla - \mathbf{A})\psi\right|^2 + \kappa^2(B - H)^2. \quad (6)$$

Here,  $H$  is the external magnetic field. Since the studies were carried out with no transport current, we applied the Coulomb gauge  $\Phi = 0$  for all times and positions. All equations were discretized following the link variable method [36], an important tool that preserves the gauge invariance of the TDGL equations.

### 2.1. Sample details

We simulated three superconducting square samples with lateral size  $L = 30\xi(0)$  with a concentric square defect of dimension  $l = 10\xi(0)$  (see the left inset of Figure 1). The discretization of equations (1 - 6) was made in a uniform mesh taking into account with five points per coherence length, i.e.,  $\Delta x = \Delta y = 0.2\xi(0)$ . Three different types of defects were considered: (i) a blind hole, which consists of a material with  $T_c$  lower than that one of the superconducting matrix; (ii) a through hole; and (iii) a material whose  $T_c$  is greater than that of the superconducting matrix, which hereafter we refer to as a *strong defect* (SD). It was also considered  $\kappa = 5$  (which refers to a Pb-In alloy) [37], and the temperature was set at  $0.5T_c$ . The external magnetic field was increased in steps of  $\Delta H = 10^{-3}H_{c2}(0)$  from  $H = 0$  to  $H = 0.5H_{c2}(0)$ . For our purposes, it was sufficient to go up to  $H = 0.216H_{c2}(0)$ .

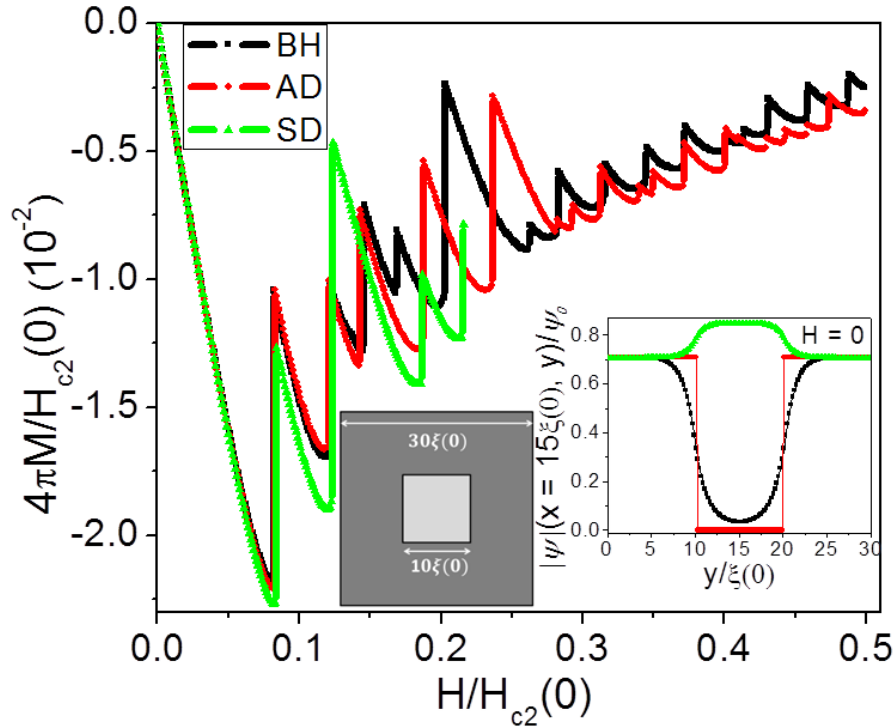


**Figure 1.** Magnetization as function of the applied magnetic field of the simulated samples. The left inset shows an schematic view of the systems, and the right inset shows the distribution of  $|\psi|$  in the middle of the samples, i.e., along the  $y$ -axis at  $x = 15\xi(0)$ .

Hereafter, the specimens will be referred by their associated defects, i.e., the BH, AD, and SD, for those with a blind hole, an antidot, and a strong defect, respectively. The effect of the nature of the defects over  $\psi$  is shown in the right inset of Figure 1. The distribution of the superconducting order parameter was taken at  $y$ -axis, and  $x = 15\xi(0)$ .

### 3. Results and discussion

#### 3.1. Equilibrium aspects - Vortex configurations

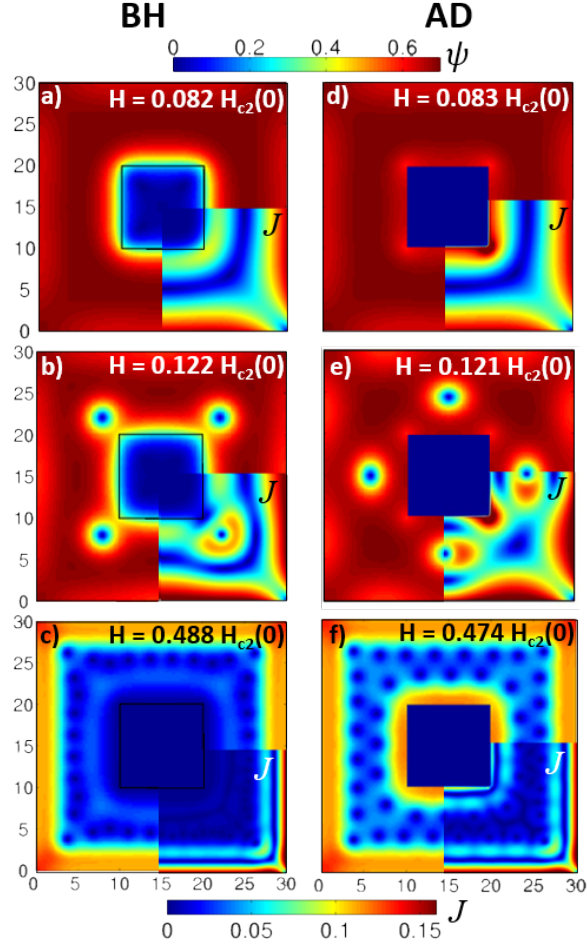


**Figure 2.** Comparison of the order parameter  $|\psi|$  between BH and AD samples for the equilibrium state of three values of the external applied field. Each of the panels also shows the distribution of the absolute value of the current density  $J$  in the samples.

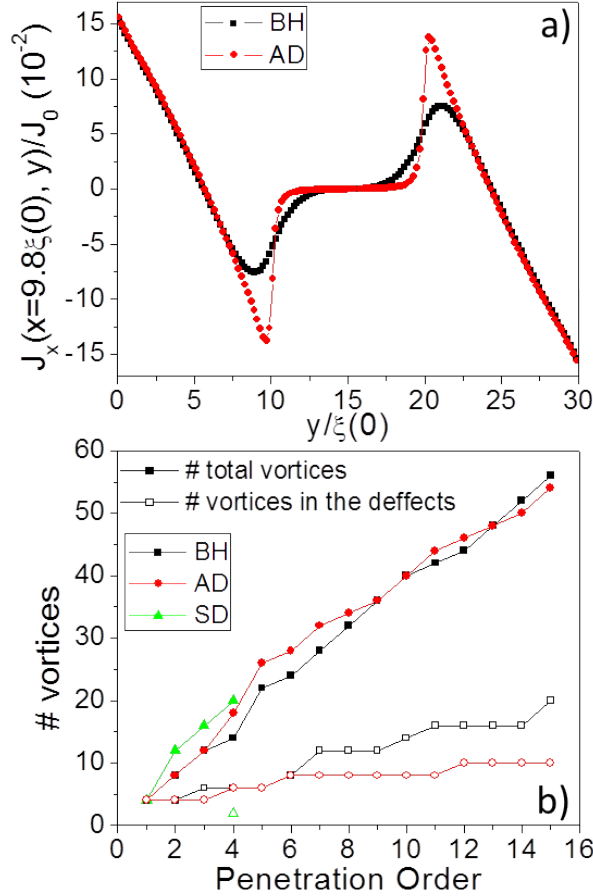
Figure 1 shows the behavior of the magnetization as a function of the applied field for the three simulated samples, each one with a different type of central defect mentioned previously. As can be seen, no matter what is the type of the defect, the lower critical field ( $H_{c1}$ ) is approximately the same, namely,  $0.082H_{c2}(0)$ ,  $0.083H_{c2}(0)$ , and  $0.084H_{c2}(0)$  for BH, AD, and SD samples, respectively. The magnetic behavior of the BH and AD samples is quite similar up to the third vortex penetration. On the other hand, the  $M(H)$  curve of the SD sample does not match with those ones of the other samples for all  $H > H_{c1}$ . It is important to mention that the nature of the defects affects the magnetic response of superconducting films. For example, flux avalanches [19, 24, 38], which are usually undesired events, can be influenced by using different types of engineered pinning as shown in Ref. [39].

Figure 2 shows snapshots of  $|\psi|$ , and the absolute value of the shielding currents,  $J$ , positioned at the fourth quadrant of each image, for both the BH and AD samples. The stationary states after the first vortex penetration are shown in panels (a) and (d). As one can see, a more degraded superconducting region takes place around the BH defect than in the vicinity of the AD one. In addition, the distribution of currents significantly changes from one type of defect to another. Moreover, the distribution of vortices inside the defects is rather different. While in the AD sample, the flux is continuously distributed into the defect. In the other case, they seem to be spread inside the BH. Just after the second penetration at  $H = 0.122H_{c2}(0)$  for BH sample, and  $H = 0.121H_{c2}(0)$  for AD one, four more vortices are found at the vertices of the defect for the former case, whereas they are positioned in the midpoint of the square of the later one (see panels (b) and (c)). This can be explained by the fact that the current density is much larger for the AD than for the BH. Such current crowding effect [40] will be discussed in more details latter on. Finally, the last analyzed penetration occurred at  $H = 0.488H_{c2}(0)$  for BH, and  $H = 0.474H_{c2}(0)$  for AD samples. Up to this stage, BH and AD samples accumulate 56 and 54 penetrated vortices, respectively. Although these numbers are similar, the BH defect presents twice as many vortices (20) as the AD one. This result is in opposition to what was found in Ref. [19]. However, we must emphasize that in this work, the authors considered an infinite film with a regular array of defects. This points out that, in mesoscopic materials, smooth surfaces between the superconducting region and the defect create a lower barrier to the penetration of more vortices in a BH than in an AD.

Still concerning Figure 2 another import remark must be stressed. From panels (c) and (f) we can observe that around the BH, the superconductivity is suppressed, and the vortices are disposed of in a shell-like structure (panel (c)). On the other hand, for the AD sample (panel (f)), the superconductivity is more preserved around the defect, and the vortices are distributed in two rows forming a near triangular lattice.

In panel (a) of Figure 3 is shown the  $x$ -component of the current density of the superconducting current along the  $y$ -axis for the fixed value of  $x = 9.8\xi(0)$  immediately after the first penetration of vortices for both BH and AD samples. First, notice that the defects' currents circulate opposite to the shielding ones at the samples' borders, as expected. As can be seen, the intensity of  $J_x$  is more significant for the AD defect by showing a sharper distribution near the edge of the defect. Such behavior implies in a stronger repulsive interaction with external vortices than that one presented by the BH. In panel (b) of Figure 3, we exhibit the total number of vortices in the samples after each vortex penetration. All systems, the mixed state sets in with vorticity four (4 vortices), which means that this first event is only due the the geometry of the sample. The subsequent penetrations show that both the geometry and the characteristic of the defects are essential to control the configuration of vortices.

Such behavior could be understood by looking at the distribution of  $J$  in Meissner state, which is shown in Figure 4, for  $H = 0.070H_{c2}(0)$ . In panel (a) it is shown the current density distribution as a function of  $y$  for  $x = 9.8\xi(0)$ , i.e., along a line very



**Figure 3.** (a) Variation of the  $J_x$  as a function of  $y$  for  $x = 9.8\xi(0)$ . The current at the edges of the defects is more significant and sharper for the AD. (b) The closed symbols represent the total vorticity in the samples in each penetration event, and the open symbols show the vorticity of the defects.

close to the border of the defect. It can be seen that the current changes smoothly near the edge of the BH defect, whereas for the AD one,  $J$  presents a dramatic variation near the corner, signaling a very strong current crowding [40]. In panel (b) of Figure 4 it is shown the variation of  $J$  along a middle line  $x = 15\xi(0)$ , going through the defects. As expected, while  $J$  suddenly drops to zero inside the AD, it goes smoothly to zero at the BH. However, for SD,  $J$  presents a local minimum outside the defect and a linear dependence on its position.

The behavior of  $J$  in the SD defect explains the late penetration of vortices inside it compared to the BH and AD defects. As such, defect presents better superconducting properties (higher  $T_c$  and  $J$ ) than the surrounding material, a substantial magnetic pressure must be applied to move the vortices in the matrix (which acts as a vortex reservoir) to the SD region. Figure 5 shows snapshots of  $|\psi|$  for different values of  $H$ . Only for  $H = 0.216H_{c2}(0)$  the first penetration of vortices will penetrate the SD defect.



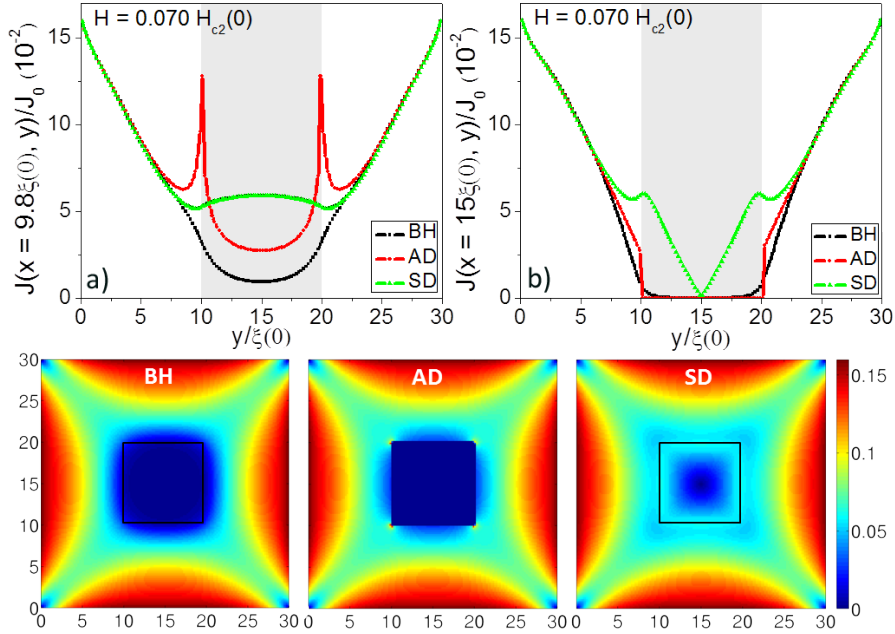


**Figure 4.** Superconducting current density as a function of the position in the Meissner state for  $H = 0.070H_{c2}(0)$ . (a) Variation of  $J$  along the  $y$ -axis for  $x = 9.8\xi(0)$  (a line close to the edge of the defects). (b) Variation of  $J$  along the middle line  $x = 15\xi(0)$ . Below these two panels, it is shown the snapshots of  $J$  for all the simulated samples. The red dots on the vertices of the AD defect indicate the current crowding effect at these points. For SD,  $J$  presents a local minimum in the defect's vicinity and a linear dependence as a function of the position inside it.

### 3.2. Non-equilibrium aspects - Characterization of the vortex dynamics

By the out of the equilibrium states, one can study the vortex dynamics by analyzing the temporal behavior of the induced voltage  $V(t)$ , magnetization  $M(t)$ , and free energy  $E(t)$ . The main panel of Figure 6 shows  $V(t)$  and  $M(t)$  for the vortex penetration at  $H = 0.488H_{c2}(0)$  in BH sample. The inset shows the  $E(t)$  behavior. The time, in picoseconds, was calculated taking into account a Pb-In alloy, with  $T_c = 7$  K and  $\kappa = 5$ . The  $V(t)$  curve is directly related to the vortex motion and accommodation. The voltage increases with the vortex nucleation, as can be seen in snapshots I, II, and III reaching a maximum value,  $V = 2.85 \times 10^{-2}V_0$ , with the complete vortex penetration ( $t = 33$  ps). However, the strong repulsive interaction with the inner vortices (see snapshot IV) slows down the penetrating vortices leading  $V(t)$  to a quick drop. After that, a small valley at  $t = 34$  ps with a negative  $V(t)$  ( $V = -0.54 \times 10^{-2}V_0$ ) takes place. Such behavior is related to an accommodation of the vortices (exemplified by the snapshots V and VI in Figure 5).

Still in Figure 6 is noticed a delay of  $M(t)$  response comparing to the  $V(t)$  one. The magnetization is also non-sensitive to the vortex accommodation. The filled squares curve in Figure 6 shows the  $M(t)$  response where a peak is evidenced as a consequence of the vortex penetration. The inset at the same figure shows the minimization of

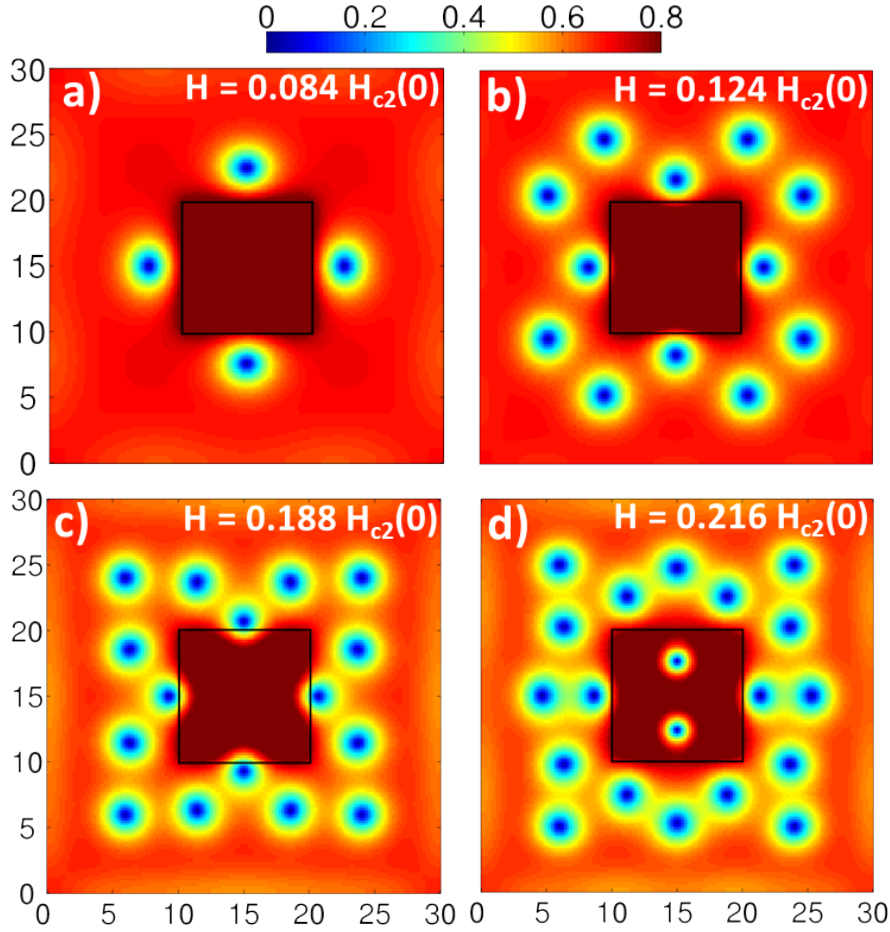


**Figure 5.** Superconducting order parameter  $|\psi|$  in the equilibrium state of the first four vortex penetrations in the SD sample. (a) First vortex penetration in the sample at  $H = 0.084H_{c2}(0)$ ; (b) second vortex penetration at  $H = 0.124H_{c2}(0)$ ; (c) third vortex penetration at  $H = 0.188H_{c2}(0)$ ; (d) fourth vortex penetration in the sample at  $H = 0.216H_{c2}(0)$ .

the free energy after the vortex penetration, and it is also non-sensitive to vortex accommodations. The AD sample presents a similar behavior, and it is not shown here.

The penetration dynamics at  $H = 0.216H_{c2}(0)$  is shown in Figure 7 for the SD sample. It is noticed qualitative changes in  $V(t)$ ,  $M(t)$ , and  $E(t)$  responses in comparison with the results for BH and AD samples. In such a case, the  $V(t)$  presents two peaks. The first at  $t = 59$  ps ( $V = 8.82 \times 10^{-2}V_0$ ) is associated with the penetration of four vortices as shown in the snapshot I and II. The second peak at  $t = 195$  ps ( $V = 0.87 \times 10^{-2}V_0$ ) is due to the penetration of two vortices in the defect, as shown by the sequence of snapshots from III to VI. The  $M(t)$  increases with the penetration of the four other vortices, followed by a meta-stable equilibrium characterized by a plateau of about 100 ps. After that, a transition to a steady-state occurs with vortex penetration into the defect. Besides that, those meta-stable and stable vortex configuration occurs due to a minimization of  $E(t)$ , which also shows two plateaus.

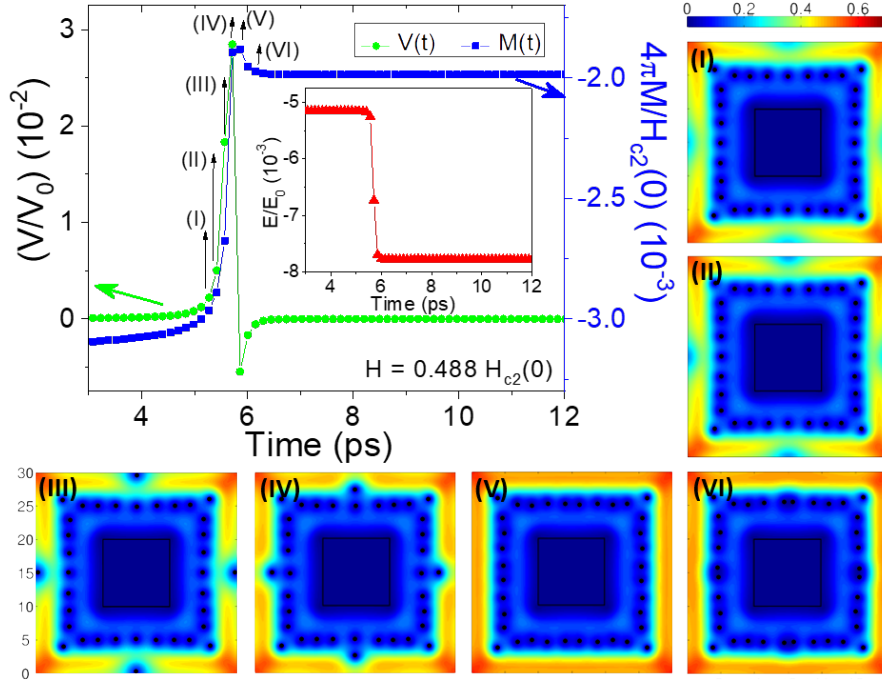


**Figure 6.** Time evolution of the induced voltage  $V(t)$ , magnetization  $M(t)$ , and free energy  $E(t)$  for the BH sample at  $H = 0.488H_{c2}(0)$ . The snapshots of  $\psi$ , enumerated from (I) to (VI), show the configuration of vortices along their dynamics.

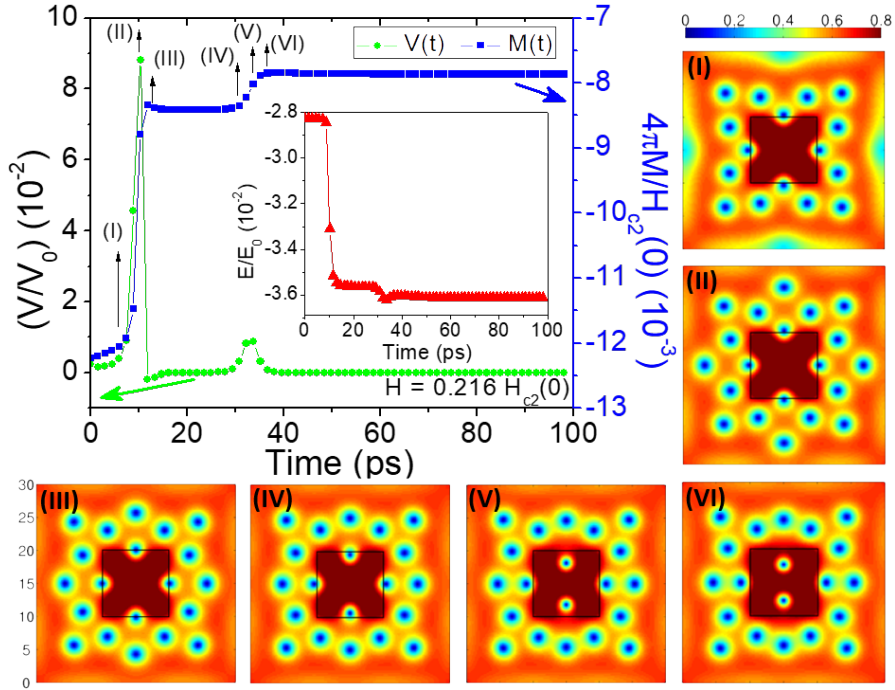


**Figure 7.** Time evolution of the induced voltage  $V(t)$ , magnetization  $M(t)$ , and free energy  $E(t)$  for the SD sample at  $H = 0.216H_{c2}(0)$ . The snapshots of  $\psi$ , enumerated from (I) to (VI), show the configuration of vortices for some instants.

The time evolution of some physical properties of superconducting systems such as  $V(t)$ ,  $M(t)$ , and  $E(t)$  is a good tool to study the vortex dynamics. One possible way to capture experimentally the penetration and motion of vortices is preparing a superconducting film decorated with the corresponding defect by adding an adjacent metallic layer. Then, potential leads are connected to a voltmeter with time resolution and voltage scale to monitor the signal in this normal layer, as presented in Figure 8. Once vortex motion occurs, the variation of magnetic flux induces eddy currents in the metal and a voltage pulse is measured. However, the time dependence of the induced electrical voltage in the metallic layer is not exactly the same as shown in Figures 6 and 7 due to the variation of the applied magnetic field. A similar superconductor-metal hybrid was prepared by P. Mikheenko and co-authors [41] to obtain the velocity of flux avalanches, which is composed by a bunch of magnetic flux with extremely high velocities (as high as 100 km/s). Therefore, the voltage signal of some vortices is somehow far more challenging.

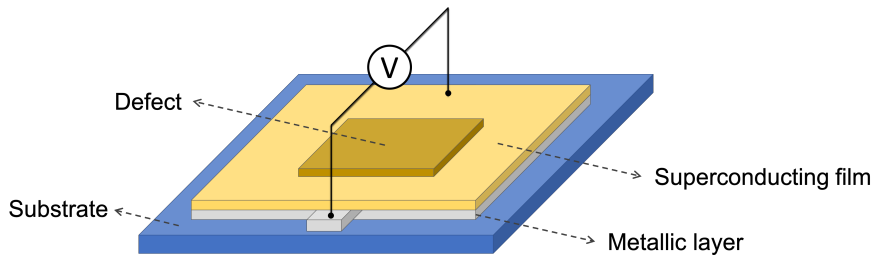


**Figure 8.** Suggestion of an experimental apparatus to monitor the vortex motion in a decorated superconducting film. A metallic layer coupled to a voltmeter is added to the system and the voltage pulse as a consequence of vortex motion is captured.

#### 4. Conclusion

We studied the effect of pinning centers of different natures on the vortex matter in mesoscopic superconductors. It was shown that  $H_{c1}$  (the field for the first penetration) does not depend on the defect's nature. However, the following penetrations result from the competing currents distribution, i.e., the interaction between the shielding currents and the currents surrounding the defects. Such a fact also plays an essential role in the vortex arrangement in the superconducting region. Also, the crowding of the currents produces a less degraded superconducting region around the antidot, contrasting with a blind hole. Such a remaining superconducting region could drive the sample with an antidot to support a higher  $H_{c2}$  than samples with blind holes. Besides, more vortices populate the sample with a defect made of a superconductor with higher  $T_c$  (strong defect) at the first penetrations. This defect could protect the inner material and control the vortex dynamics with more accuracy in that region. It was also shown that  $M(t)$  is not sensitive to vortex accommodation but indicates the penetrations in the strong

defect. On the other hand,  $V(t)$  is sensitive to vortex penetration and accommodation, an alternative tool for studying vortex dynamics in mesoscopic superconducting systems.

## Acknowledgments

We thank the Brazilian Agencies São Paulo Research Foundation (FAPESP), grants 2016/12390-6, 2018/06575-9, and 2020/10058-0, Coordenação de Aperfeiçoamento de Pessoal de Nível Superior - Brasil (CAPES) - Finance Code 001, National Council of Scientific and Technological Development (CNPq, grant 302564/2018-7).

## References

- [1] Blatter G, Feigel'man M V, Geshkenbein V B, Larkin A I and Vinokur V M 1994 Rev. Mod. Phys. **66**(4) 1125–1388 URL <https://link.aps.org/doi/10.1103/RevModPhys.66.1125>
- [2] Campbell A and Evetts J 1972 Advances in Physics **21** 199–428 (*Preprint* <https://doi.org/10.1080/00018737200101288>) URL <https://doi.org/10.1080/00018737200101288>
- [3] Kwok W, Welp U, Crabtree G, Vandervoort K, Hulscher R and Liu J 1990 Physical review letters **64** 966
- [4] Vargas J L and Larbalestier D C 1992 Applied physics letters **60** 1741–1743
- [5] Pande C and Suenaga M 1976 Applied Physics Letters **29** 443–444
- [6] Martin J I, Vélez M, Nogués J and Schuller I K 1997 Physical review letters **79** 1929
- [7] Martin J I, Vélez M, Hoffmann A, Schuller I K and Vicent J 1999 Physical review letters **83** 1022
- [8] Moshchalkov V, Baert M, Metlushko V, Rosseel E, Van Bael M, Temst K, Bruynseraede Y and Jonckheere R 1998 Physical Review B **57** 3615
- [9] Weiss D, Richter K, Vasiliadou E and Lütjering G 1994 Surface science **305** 408–418
- [10] Silhanek A, Van Look L, Jonckheere R, Zhu B, Raedts S and Moshchalkov V 2005 Physical Review B **72** 014507
- [11] Harada K, Kamimura O, Kasai H, Matsuda T, Tonomura A and Moshchalkov V 1996 Science **274** 1167–1170
- [12] Silhanek A, Raedts S and Moshchalkov V 2004 Physica C: Superconductivity **404** 345–349
- [13] Berdiyrov G, Milošević M and Peeters F 2009 New Journal of Physics **11** 013025
- [14] Bezryadin A, Ovchinnikov Y N and Pannetier B 1996 Physical Review B **53** 8553
- [15] Reichhardt C and Grønbech-Jensen N 2000 Physical review letters **85** 2372
- [16] Shaw G, Banerjee S, Tamegai T and Suderow H 2016 Superconductor Science and Technology **29** 065021
- [17] Horng L, Cao R, Wu T C, Yang S, Wang S H, Wu J C and Yang T J 2013 Journal of Applied Physics **113** 17E118
- [18] Raedts S, Silhanek A, Van Bael M and Moshchalkov V 2004 Physical Review B **70** 024509
- [19] Raedts S, Silhanek A, Van Bael M, Jonckheere R and Moshchalkov V 2004 Physica C: Superconductivity **404** 298–301
- [20] Palacios J 1998 Physical Review B **58** R5948
- [21] Palacios J 1998 Physica B: Condensed Matter **256** 610–617
- [22] Geurts R, Milošević M and Peeters F 2010 Physical Review B **81** 214514
- [23] Pereira P J, Chibotaru L F and Moshchalkov V V 2011 Physical Review B **84** 144504
- [24] Brisbois J, Gladilin V N, Tempere J, Devreese J T, Moshchalkov V V, Colauto F, Motta M, Johansen T H, Fritzsche J, Adami O A, Nguyen N D, Ortiz W A, Kramer R B G and Silhanek A V 2017 Phys. Rev. B **95**(9) 094506 URL <https://link.aps.org/doi/10.1103/PhysRevB.95.094506>
- [25] Pinheiro L B L G, Caputo M, Cirillo C, Attanasio C, Johansen T H, Ortiz W A, Silhanek A V and

- Motta M 2020 Low Temperature Physics **46** 365–371 (*Preprint* <https://doi.org/10.1063/10.0000868>) URL <https://doi.org/10.1063/10.0000868>
- [26] Sadovskyy I A, Wang Y, Xiao Z L, Kwok W K and Glatz A 2017 Physical Review B **95** 075303
- [27] Fiory A T, Hebard A F and Somekh S 1978 Applied Physics Letters **32** 73–75 (*Preprint* <https://doi.org/10.1063/1.89845>) URL <https://doi.org/10.1063/1.89845>
- [28] Navarro E, Monton C, Pereiro J, Basaran A C and Schuller I K 2015 Physical Review B **92** 144512
- [29] Gillijns W, Silhanek A and Moshchalkov V 2007 Applied physics letters **91** 202510
- [30] Carreira S J, Chliotte C, Bekeris V, Rosen Y, Monton C and Schuller I K 2014 Superconductor Science and Technology **27** 085007
- [31] Berdiyrov G, Misko V, Milošević M, Escoffier W, Grigorieva I and Peeters F 2008 Physical Review B **77** 024526
- [32] Schmid A 1966 Phys. kondens. Materie **5** 302–317
- [33] Gor'kov L P and Eliashberg G M 1968 Sov. Phys. JETP **27** 328–334
- [34] Vodolazov D Y 2000 Phys. Rev. B **62** 8691
- [35] D Y Vodolazov I L M and Brandt E 2003 Physica C **384** 211–226
- [36] Gropp W D, Kaper H G, Leaf G K, Levine D M, Palumbo M and Vinokur V M 1996 Journal of Computational Physics **123** 254–266
- [37] Poole C P, Farach H A and Creswick R J 1995 Superconductivity (Academic Pr)
- [38] Silhanek A V, Raedts S and Moshchalkov V V 2004 Phys. Rev. B **70**(14) 144504 URL <https://link.aps.org/doi/10.1103/PhysRevB.70.144504>
- [39] M I Montero J J Akerman A V and Schuller I K 2003 Europhysics Letters **63** 118–124
- [40] Clem J R and Berggren K K 2011 Phys. Rev. B **84**(17) 174510 URL <https://link.aps.org/doi/10.1103/PhysRevB.84.174510>
- [41] Mikheenko P, Qviller A J, Vestgård J I, Chaudhuri S, Maasilta I J, Galperin Y M and Johansen T H 2013 Applied Physics Letters **102** 022601 (*Preprint* <https://doi.org/10.1063/1.4775693>) URL <https://doi.org/10.1063/1.4775693>